scientific reports

Check for updates

OPEN

Plasma exosomes from patients with coronary artery disease promote atherosclerosis via impairing vascular endothelial junctions

Jian Han[1], Xiaoyan Kang[1], Yazhen Su[1], Jing Wang[2], Xiaogang Cui[2], Yunfei Bian[3] & Changxin Wu[2]✉

The underlying mechanism of vascular endothelial hyperpermeability caused by decrease of endothelial junctions occurring in atherosclerosis remains elusive. Our findings identified that plasma exosomes from patients with stable coronary artery disease (Exo^{SCAD}) contain differentially expressed miRNAs that are clustered with genes related to cell junctions, prompting us to investigate the role of Exo^{SCAD} in regulating vascular endothelial junctions and to elucidate the underlying mechanisms. Here, we show that Exo^{SCAD} markedly impair vascular endothelial junctions via suppressing VE-Cadherin and ZO-1 in endothelial cells in vitro and in vivo, consequently increases endothelial permeability. Critically, exosomal miR-140-3p plays a crucial role in Exo^{SCAD}-induced inhibition of ZO-1, and may be an important causative factor in the development of endothelial hyperpermeability during atherosclerosis. Additionally, exosomal miR-140–3p level coordinates with severity of SCAD. Targeting miR-140-3p in circulating exosomes might open novel options for treatment of atherosclerosis.

Keywords Stable coronary artery disease, Plasma exosomes, miR-140-3p, Atherosclerosis, Endothelial cell junctions

Coronary artery disease (CAD), which can be classified into stable coronary artery disease (SCAD) and acute coronary syndrome (ACS), poses great threat to human health due to its high morbidity and mortality[1]. It is noteworthy that SCAD will develop to ACS if it cannot be timely and effectively controlled, resulting in an enhanced risk of severe and death of patients[2]. Atherosclerosis, the pathogenesis of which includes endothelial damage, lipid accumulation, inflammatory cell adhesion, plaque formation and rupture, is the pathological basis of CAD[3]. However, the methods to prevent and treat atherosclerosis are still limited due to the lack of an in-depth understanding of its pathogenesis. Consequently, it is of great significance to explore the pathogenesis of atherosclerosis in order to determine novel and effective therapeutic targets.

Exosomes, a type of nanoscale extracellular vesicles secreted from various cell types, can regulate various physiological and pathological processes through mediating intercellular communication[4]. Mounting evidences in recent years have found that miRNAs, as a main component of exosomes[5], are crucial mediators for exosomes to perform biological functions[6,7]. Exosomal miRNAs have been demonstrated to be involved in the occurrence and development of various vascular diseases, including atherosclerosis[8]. For example, small cell lung cancer cells-secreted exosomal miR-141 and hypoxic papillary thyroid cancer cells-derived exosomal miR-181a aggravate tumor angiogenesis and growth via promoting endothelial cells (ECs) proliferation, invasion, migration and tube formation[9,10]. Exosomal miRNA-9-3p derived from the vitreous humor of proliferative diabetic retinopathy patients promotes proliferation, migration and tube formation of primary human retinal ECs[11]. M1-like macrophage-derived exosomal miR-155 reportedly leads to inhibition of angiogenesis and exacerbation of cardiac dysfunction via modulating its target genes[12]. Notably, vascular smooth muscle cells-

[1]Shanxi Bethune Hospital, Shanxi Academy of Medical Sciences, Third Hospital of Shanxi Medical University, Tongji Shanxi Hospital, Taiyuan 030032, Shanxi, China. [2]Key Lab of Medical Molecular Cell Biology of Shanxi Province, Institutes of Biomedical Sciences, Key Laboratory of Chemical Biology and Molecular Engineering of Ministry of Education, Shanxi University, Taiyuan 030006, Shanxi, China. [3]Department of Cardiology, The Second Hospital of Shanxi Medical University, Taiyuan 030001, Shanxi, China. ✉email: cxw20@sxu.edu.cn

derived exosomal miR-221/222 from diabetic sources were confirmed to promote vascular inflammation and atherogenesis[13].

In recent years, the roles of exosomal miRNAs in circulation have been widely studied and found to be function crucially in atherosclerosis[14,15]. As an illustration, serum exosomal miR-143 and miR-126-3p from patients with myocardial infarction promote atherosclerosis through IGF-IR and TSC1/mTORC1/HIF-1α pathway, respectively[16,17]. Based on our previous small RNA sequencing (RNA-Seq) results, a total of 244 miRNAs (29 up-regulated and 215 down-regulated) were identified to be potentially differentially expressed in plasma exosomes of SCAD patients (Exo^{SCAD}) in comparison with control subjects (Fig. 1A). Functional enrichment analyses identified these differentially expressed miRNAs (DEmiRNAs) to be clustered with genes associated with cell junctions, cytosol, dendritic spine, glutamatergic synapse, postsynaptic density, among which cell junctions that are critical in regulating vascular endothelial permeability[18–20] showed relatively most significant abundant (Fig. 1B). More importantly, the increased vascular endothelial permeability mediated by impaired endothelial cell junctions is the key step for lipid and leukocyte to cross the vascular endothelial barrier and deposit in the subendothelial layer in early atherosclerosis[21–23].

It was reported that exosomal miRNAs secreted from highly metastatic cancer cells increase endothelial permeability and facilitate tumor metastasis by targeting endothelial junctional proteins[24,25]. Besides, pericyte-derived exosomal miR-210-5p regulates endothelial permeability through suppressing JAK1/STAT3 signaling[26]. These prompted us to suggest that the altered Exo^{SCAD}-contained miRNAs may deteriorate endothelial permeability and promote atherogenesis through regulation of endothelial cell junctions. In a bid to determine plasma derived exosomal miRNAs that facilitate atherosclerosis via disrupting endothelial junctions, we identified that miR-140-3p highly expressed in Exo^{SCAD} could be transferred into ECs and induced endothelial hyperpermeability through suppressing the expression of zonula occludens 1 (ZO-1). Significantly, our findings illustrate that plasma exosomal miRNAs may play crucial roles in atherosclerotic pathophysiology.

Materials and methods

Collection of plasma samples

Plasma samples from 39 patients with SCAD and 39 paired healthy controls were prospectively collected (clinical characteristics are summarized in Table S1) from January to June 2022 at the Second Hospital of Shanxi Medical University in Taiyuan, China. The following are the primary inclusion criteria for the SCAD group[27]: (1) A luminal stenosis of at least 50% in the left main stem or at least 70% in no less than one major coronary arteries. (2) The pain or discomfort in the chest persists for less than 10 min. Healthy controls were selected based on age- and sex-matched being adults with no clinical signs of CAD and normal ECG results. Subjects with inflammation, infection, autoimmune diseases, severe hepatic or renal dysfunction, or a history of malignancy diseases were eliminated. All experiments were approved by the Ethics Committee of The Second Hospital of Shanxi Medical University, and performed following the Declaration of Helsinki. Informed consent was obtained from all the participants.

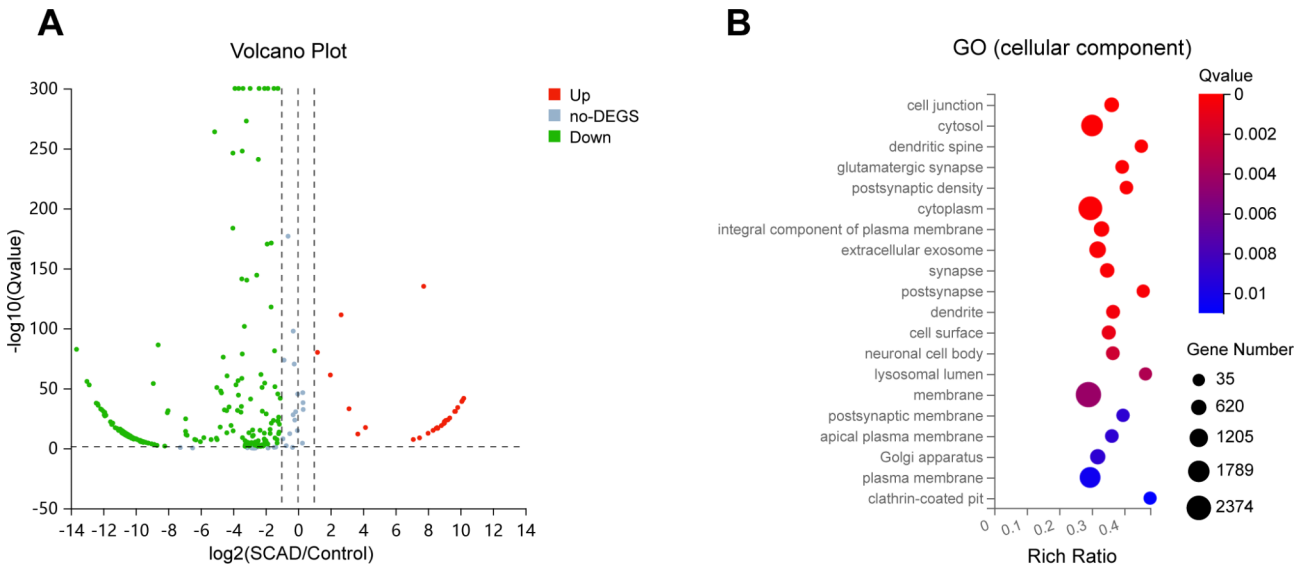

Fig. 1. Plasma exosomal DEmiRNAs identified by small RNA-Seq in patients with SCAD and the corresponding GO (cellular component) enrichment analysis. (**A**) Plasma exosomal statistically significant DEmiRNAs in patients with SCAD ($n=3$) in comparison with healthy controls ($n=3$). DEmiRNAs up-regulated and down-regulated with statistical significance are represented by the red and green points, respectively. (**B**) Enrichment analysis of GO (cellular component) presenting the most abundant cellular components associated with these DEmiRNAs target genes. no-DEGS: not differentially expressed genes; SCAD: stable coronary artery disease; GO: Gene Ontology; DEmiRNAs: differentially expressed miRNAs.

Extraction, identification and quantification of plasma exosomes

To remove cells and cell debris, plasma underwent a series of centrifugation (300 ×g for 10 min, 2000×g for 10 min and 10,000 ×g for 30 min). After being filtered by a 0.22 μm filter membrane (Millipore), the supernatant underwent additional ultracentrifugation for 5 h at 110,000×g (CP100NX, HITACHI, Tokyo, Japan). The precipitates were washed 1 time with PBS by ultracentrifugation at 110,000×g for another 5 h. Exosome samples were resuspended by adding 200 μL PBS. The exosome suspension (10 μL) was then added onto a copper grid coated with formvar for 15 min before adding a 2% phosphotungstate solution (10 μL) for 1 min. After blotting the residual liquid by filter paper, the copper grids were then observed under an transmission electron microscope (HT-7800, HITACHI, Tokyo, Japan) at 100 kV. The exosome suspension (30 μL) was analyzed for nanoparticle tracking analysis using NanoFCM (Flow NanoAnalyzer, Xiamen, China). To measure the protein concentration of the isolated exosomes, a bicinchoninic acid protein assay kit (Solarbio, Beijing, China) was utilized. The cholesterol content of the exosome preparations was measured using the Amplex Red Cholesterol Assay Kit (Invitrogen, USA) according to the manufacturer's instructions. For cell treatment, an addition of exosomes (approximately 2 μg) to 2×10^5 recipient cells was performed, as described in a previous report[28]. For in vivo administration, recipient mice were intravenously injected with 100 μg of exosomes every 3 days for 4 weeks as previously reported[29].

Cell culture

Human aortic endothelial cells (HAECs; Sciencell, USA) were grown in an endothelial cell medium supplemented with 10% exosome-depleted FBS (prepared through ultracentrifugation for 8 h at 110,000×g), ECs growth supplement (ScienCell, USA), 100 μg/mL streptomycin sulphate and 100 U/mL penicillin sodium (Hyclone, USA), at 37°C in humidified air containing 5% CO_2.

Uptake of exosomes by HAECs

The exosome preparation was labeled by PKH26 (Sigma-Aldrich, USA). Briefly, exosome preparation and 2 μL of PKH26 were resuspended in 1 ml Diluent C, respectively. The exosome suspension was then added to the PKH26 solution and incubated for 5 min before adding 0.5% bovine serum albumin to stop the staining. The labeled exosomes were ultracentrifuged at 110,000 g at 4°C for 70 min and then resuspended by adding 200 μL PBS before filtering by a 0.22 μm filter membrane (Millipore, USA). The HAECs at 80% confluence were exposed to the labeled exosomes for 12 h. The nuclei were stained by using DAPI (Beyotime, Shanghai, China) for 5 min before imaging under a confocal microscope (LSM710, Carl Zeiss, Oberkochen, Germany).

Cell and exosome transfection

The miR-140-3p agomir (agomir-140-3p), miR-140-3p antagomir (antagomir-140-3p), and their negative controls were synthesized by RiboBio (Guangzhou, China). HAECs were transfected with RNA duplex (50 nM) or miRNA antagomir (100 nM) using lipofectamine 3000 (Invitrogen, USA) following the manufacturer's guidelines. Briefly, the lipofectamine 3000/RNA complexes were prepared in OptiMEM (Invitrogen, USA) and then incubated with HAECs for 8 h before replacing the medium with fresh medium supplemented with 10% exosome-deleted FBS for further treatment. Transfection of antagomir-140-3p/NC into exosomes was performed using Exo-Fect Exosome Transfection Kit (System Biosciences, USA) according to the manufacturer's guidelines.

Endothelial permeability assay

For endothelial permeability analysis, HAECs (2×10^4) were grown on the upper chamber of a 24-well transwell inserts (0.4 μm pore size; Corning, USA) and allowed to reach a monolayer cell barrier at 100% confluence, followed by addition of PBS, Exo^{SACD}, Exo^{HC} or Lipopolysaccharide (10 μg/ml) and continued culture for 48 h. Rhodamine B isothiocyanate dextran (rhodamine-dextran, average MW 70,000; Sigma, USA) at a concentration of 20 mg/mL was added into the upper chamber. The amount of rhodamine-dextran in the bottom well was quantified to assess the endothelial permeability. Briefly, 40 μL medium in the bottom well was taken out at 30 min, 60 min and 90 min and analyzed by using a SpectraMax microplate reader (excitation at 488 nm, emission at 525 nm; SpectraMax M5, Molecular Devices, USA).

Western blot assay

The exosome suspension or cells were lysed on ice using RIPA buffer (Solarbio, Beijing, China) containing PMSF, and the protein concentrations were determined using a bicinchoninic acid protein assay kit (Solarbio, Beijing, China). Protein lysate was separated by SDS-PAGE and transferred onto polyvinylidene fluoride membranes, which were subsequently blocked for 2 h at 4°C and incubated with primary antibodies overnight at 4°C, then incubated with the peroxidase-conjugated secondary antibodies (1:5000 dilution; Bioss, Beijing, China) for 1 h at 37°C. Protein bands were visualized using a chemiluminescence reagent (Abbkine, Wuhan, China). First antibodies used in the experiment were as follows: anti-ZO-1 (1:1000 dilution; Abcam, ab276131), anti-VE-Cadherin (1:1000 dilution; Abcam, ab33168), anti-CD81 (1:1000 dilution; Abcam, ab109201), anti-CD63 (1:1000 dilution; Abcam, ab134045), anti-CD9 (1:1000 dilution; Abcam, ab236630), anti-Calnexin (1:1000 dilution; Abcam, ab133615), and anti-Apolipoprotein B (1:1000 dilution; Abcam, ab312318).

Reverse transcription quantitative real-time polymerase chain reaction

Total RNA from exosomes or cells/tissues was extracted using exoRNeasy Serum/Plasma Midi Kit (Qiagen, Hilden, Germany) or Trizol (Invitrogen, USA), respectively. After purification and quantification, the reverse transcription of RNA into cDNA was performed using a miRcute Plus miRNA First-Strand cDNA Kit (Tiangen, Beijing, China). A miRcute Plus miRNA qPCR Kit (SYBR Green) (Tiangen, Beijing, China) was used to perform

real-time reactions following the manufacturer's instructions. The relative expression levels of miRNAs were normalized to U6 and calculated using the $2^{-\Delta\Delta CT}$ method. The primer sequences are presented in Table S2.

Luciferase reporter assay

The predicted miR-140-3p binding site in the 3'-UTR of human ZO-1 sequence and its mutant were cloned into a luciferase reporter vector. Next, reporter vectors (wild-type or mutant) with either the agomir-140-3p/antagomir-140-3p or their negative controls at three different concentrations (25 nM, 50 nM, 100 nM) were co-transfected into HEK293T cells using lipofectamine 3000 (Invitrogen, USA) and cultured for 48 h. Firefly luciferase activity normalized to Renilla luciferase activity was analyzed using a dual-luciferase reporter assay system (Promega, USA) following the manufacturer's protocol. The luciferase activities were measured using a SpectraMax microplate reader (SpectraMax M5, Molecular Devices, USA).

Animal models

Male $ApoE^{-/-}$ mice aged 8 weeks were obtained from the GemPharmatech Co., Ltd (Beijing, China), and given a high-fat diet (HFD) for 12 weeks under a specific pathogen-free environment with a 12 h:12 h light-dark cycle. Sample size determination was based on previous experience with similar studies. Four weeks after HFD feeding, mice were randomly treated with plasma exosomes (100 μg each time) or PBS via tail vein every 3 days for 4 weeks. After 12 weeks of HFD, mice were either euthanized for tissue collection and assessment, or subjected to the injection of Evans blue. All animal experiments were performed under the rules approved by the Institutional Animal Care and Use Committee of Shanxi Medical University.

In vivo vascular permeability assay

For in vivo permeability assay, 100 μL Evans blue (1% in PBS; Sigma-Aldrich, USA) was injected i.v. into the recipient mice via tail vein and sacrificed after 1 h. After a transcardiac perfusion with 10 mL PBS, aortas were then removed and imaged under a stereomicroscope after washing with PBS. Extraction of Evans blue dye from the aortas was performed by incubating the aortas in formamide at 55°C for 24 h before subjecting to centrifugation. Absorbance at 610 nm was measured to evaluate the concentration of the Evans blue in supernatant. The amount of Evans blue extravasated per milligram of artery represented vascular permeability.

Analyses of atherosclerotic lesion

The hearts with entire length of the aorta were harvested and fixed in 4% paraformaldehyde. The thoracoabdominal aortas were unfolded longitudinally and pinned on a black wax surface, followed by staining with Oil Red O (Solarbio, Beijing, China). Images were obtained with a digital camera (Canon, Tokyo, Japan) and quantifications for percent lesion area were then analyzed using ImageJ software. Hearts with aortic root were embedded in OCT and cryosectioned into 7 μm slices, followed by staining with Oil Red O. Images were obtained using a microscope (Zeiss, Oberkochen, Germany) and were quantified for percent lesion area using Image J software. Data were averaged in 3–5 sections per mouse.

Immunostaining

For immunohistochemistry staining, the sections of aorta were incubated with 3% H_2O_2 for 15 min to eliminate endogenous peroxidase. After blocking with 5% goat serum for 2 h, the samples were immunostained with anti-ZO-1 antibodies (1:250 dilution; Abcam, ab276131) or anti-VE-Cad antibodies (1:50 dilution; Abcam, ab282277) overnight at 4 °C prior to incubation with the corresponding secondary antibodies (1:200, Life Technologies, USA) for 1 h. Nuclei were visualized with hematoxylin (Beyotime, Shanghai, China). Images were recorded using a microscope (Zeiss, Oberkochen, Germany) equipped with a camera.

Statistical analyses

Data are expressed as mean ± standard error of the mean or numbers and percentages for continuous variables and categorical variables, respectively. At least three replicates were conducted in every trial group. Data normalization was examined by the Kolmogorov-Smirnov test. Statistical analyses were performed with unpaired Student's t-test or non-parametric Mann-Whitney U-test for 2-group comparisons using GraphPad Prism 8.0 (GraphPad Software Inc). Categorical variables were assessed using the Chi-square test or Fisher's exact test. Relationships between continuous variables were analyzed by using Spearman's correlation analysis. p values < 0.05 were considered statistically significant.

Results

Plasma exosomes are taken up by HAECs

Vesicles isolated from plasma exhibited a bilayer membrane structure under transmission electron microscope (Fig. 2A) and expressed the positive markers CD9, CD63 and CD81, but not the negative marker Calnexin (Fig. 2C). Nanoparticle tracking analysis revealed that the diameters of the isolated vesicles were between 60 and 150 nm, with a average size of approximately 80 nm (Fig. 2B). To analyze the expression levels of apoB in exosomes, western blot was performed in the same protein amount of exosome preparations, which showed that the expression levels of apoB did not differ significantly between Exo^{HC} and Exo^{SCAD} (Fig. 2D). Meanwhile, no significant differences in cholesterol contents were observed between Exo^{HC} and Exo^{SCAD} (Fig. 2E). Additionally, exosomes could be internalized by HAECs under confocal microscopy, as evidenced by the images that red fluorescence was observed around the nucleus and in the cytoplasm of HAECs (Fig. 2G). Quantification of exosome distribution identified that more than 85% of HAECs were positive for PKH26 fluorescence, with no difference between the uptake of Exo^{HC} and Exo^{SCAD} (Fig. 2F).

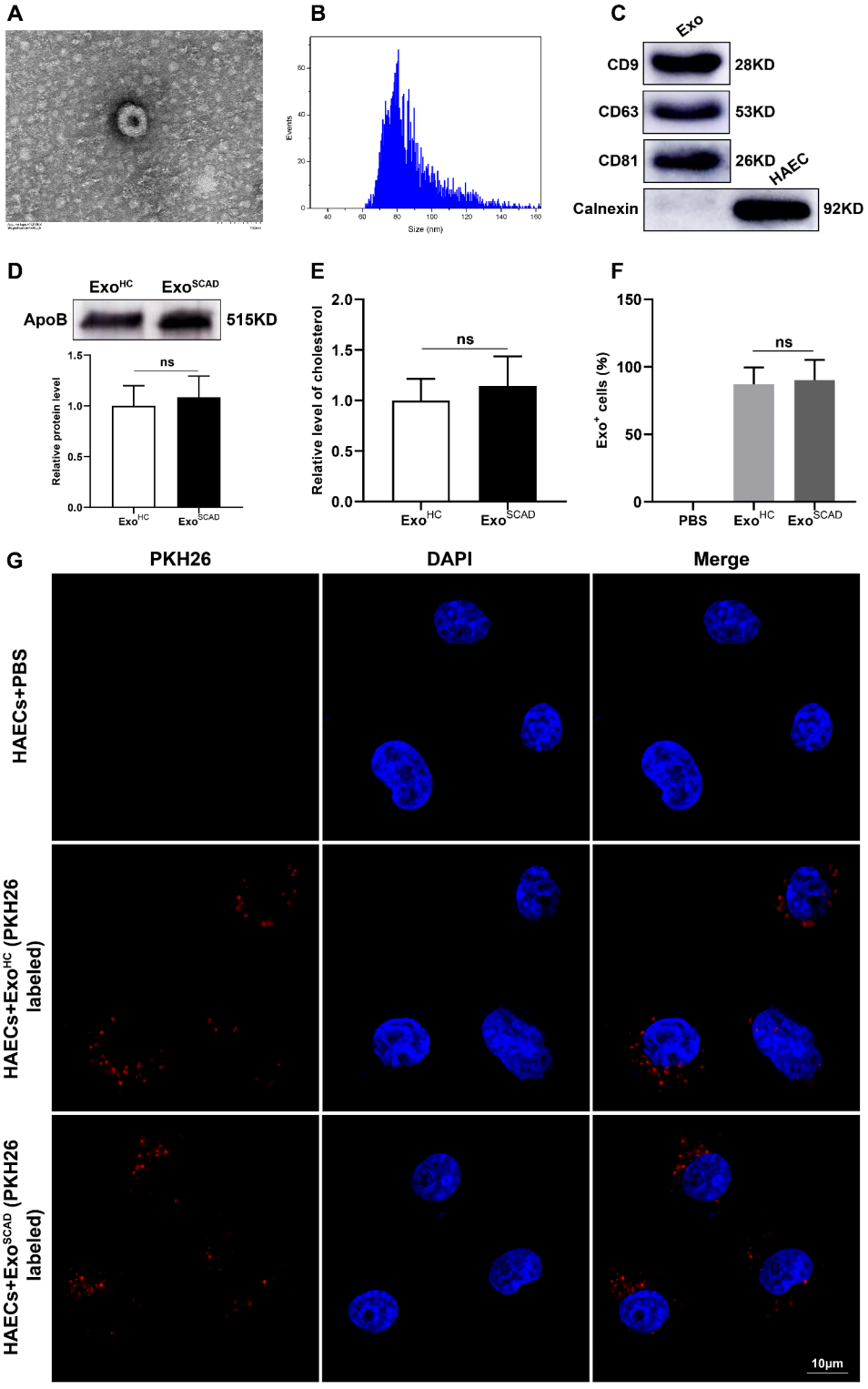

Fig. 2. Plasma exosomes identification and uptake by HAECs. (**A**) Morphological structure of the isolated vesicles by transmission electron microscope. (**B**) Particle sizes of the extracted vesicles by nanoparticle tracking analysis. (**C**) Western blot presenting the positive expressions of CD9, CD63 and CD81 in the extracted vesicles. Calnexin was negatively expressed. (**D**) Western blot presenting the expression levels of apoB (up panel) and the corresponding quantification results (down panel) in the same protein amount of exosome preparations. (**E**) Quantification of cholesterol content in Exo^{HC} and Exo^{SCAD}. (**F** and **G**) Quantification of exosome distribution by exosome-positive HAECs and representative microphotographs of HAECs incubated with PKH26-labeled plasma exosomes (red). An average of five random fields per sample were counted. Exo: exosome; HAEC: human aortic endothelial cell. Exo^{HC}: plasma exosomes of healthy controls; Exo^{SCAD}: plasma exosomes of patients with stable coronary artery disease.

Exo^{SCAD} suppress VE-cadherin and ZO-1 expressions aggravating atherosclerosis

Our previous study suggested that the most enriched cellular component in the geneontology category of the target genes of DEmiRNAs expressed in Exo^{SCAD} was cell junctions, which are crucial biomolecules in regulating vascular endothelial permeability. This prompted us to identify the potential of Exo^{SCAD} in modulating the expressions of VE-cadherin (VE-Cad) and ZO-1 that are the main component of cell junctions between ECs. Strikingly, western blot results revealed that HAECs treated with Exo^{SCAD}, but not Exo^{HC}, displayed a significant decrease of VE-Cad and ZO-1 expressions (Fig. 3A). Due to the fact that increased vascular permeability mediated by disrupted endothelial cell junctions is the critical factor that facilitate atherosclerosis, we sought to determine whether Exo^{SCAD} affect the endothelial permeability. As shown, there was significantly more dextran passed through the Exo^{SCAD}-treated HAECs monolayer in comparison with HAECs treated with PBS or Exo^{HC} ($p < 0.01$, Fig. 3B). However, endothelial permeability did not significantly differ between HAECs treated with PBS or Exo^{HC} ($p > 0.05$, Fig. 3B).

We next conducted in vivo studies in a ApoE$^{-/-}$ mouse model (atherosclerosis-prone mouse) to further identify the above-mentioned findings. ApoE$^{-/-}$ mice were fed with HFD and intravenously injected with Exo^{SCAD}, Exo^{HC} or PBS. After 12 weeks of HFD, Exo^{SCAD}-treated mice exhibited reduced protein levels of VE-Cad and ZO-1 in the aortic intima (Fig. 3C) and increased endothelial permeability ($p < 0.001$, Fig. 3D), in comparison with either Exo^{HC} or PBS-treated controls. Notably, treatment of recipient mice with Exo^{SCAD} but not Exo^{HC} or PBS resulted in a significant increase in atherosclerotic lesion area in the aorta ($p < 0.001$, Fig. 3E and F) and aortic sinus ($p < 0.001$, Fig. 3G). Meanwhile, as predicted from our in vitro results, no differences in VE-Cad and ZO-1 expressions, endothelial permeability and lesion sizes in the aortas were observed between mice treated with PBS or Exo^{HC} ($p > 0.05$, Fig. 3C–G).

Exo^{SCAD} inhibit ZO-1 expression to increase endothelial permeability via transferring highly expressed mir-140-3p into HAECs

To identify the DEmiRNAs in Exo^{SCAD} that are potentially associated with downregulation of VE-Cad and ZO−1, we sought to investigate the potential target DEmiRNAs of VE-Cad and ZO−1. Considering the inhibitory effect of miRNA on mRNA translation, we selected the 29 up-regulated exosomal miRNAs from small RNA-Seq as candidate miRNAs for further analysis. Bioinformatics analyses showed that miR−103a−3p exists the binding site of both VE-Cad and ZO−1 mRNA 3'-UTR, miR−125b−5p and miR−140−3p exist the binding site of VE-Cad and ZO−1 mRNA 3'-UTR, respectively. To further establish the expression levels of miR−103a−3p, miR−125b−5p and miR−140−3p expressed in Exo^{SCAD}, we performed reverse transcription quantitative real-time polymerase chain reaction (RT-qPCR) in a larger clinical plasma samples of subjects (including 36 SCAD patients and 36 healthy controls), which showed that miR−140−3p level was marked elevated ($p < 0.001$, Fig. 4A) in Exo^{SCAD} compared to Exo^{HC}, while miR−103a−3p and miR−125b−5p levels were unaltered ($p \geq 0.05$, Fig. 4A). Beyond that, miR-140-3p expression was significantly increased in HAECs following treatment with Exo^{SCAD}, but not Exo^{HC} ($p < 0.01$, Fig. 4B), suggesting that the highly expressed miR−140−3p can be transfered from Exo^{SCAD} into ECs. Critically, the levels of plasma exosomal miR-140-3p were positively correlated with Gensini Scores representing the severity of coronary artery stenosis of the SCAD patients ($r = 0.4391$, $p = 0.0074$, Fig. 4C).

To examine whether Exo^{SCAD}-induced downregulation of ZO−1 is through the highly expressed miR−140−3p, Exo^{SCAD} were transfected with antagomir−140−3p before adding to the HAECs. Strikingly, blockade of miR−140−3p reversed the effect of Exo^{SCAD} to inhibit ZO−1 ($p < 0.05$, Fig. 4D) and attenuated the enhanced effect of Exo^{SCAD} on endothelial permeability ($p < 0.05$, Fig. 4E). Collectively, these findings reveal that miR−140−3p highly expressed in Exo^{SCAD} is responsible for the suppressive effect of Exo^{SCAD} on ZO−1, thereby increasing endothelial permeability.

Mir-140-3p inhibits ZO-1 to increase endothelial permeability via targeting the 3′-UTR of ZO-1 mRNA

To further determine the contribution of miR-140-3p to the regulation of ZO-1 and endothelial permeability by Exo^{SCAD}, HAECs were transfected with either a agomir-140-3p or antagomir-140-3p. As shown, overexpression of miR-140-3p resulted in a down-regulated expression of ZO-1 ($p < 0.05$, Fig. 5A) and enhanced endothelial permeability ($p < 0.01$, Fig. 5B) in HAECs. Conversely, antagonism of miR-140-3p enhanced the ZO-1 expression ($p < 0.05$, Fig. 5A) and decreased endothelial permeability ($p < 0.01$, Fig. 5B) in HAECs, suggesting that miR-140-3p may regulate ZO-1 expression and endothelial permeability in ECs. Dual-luciferase reporter assay was then performed to investigate how miR-140-3p expressed in Exo^{SCAD} inhibits ZO-1 in HAECs. As shown in Fig. 5C, the activity of firefly luciferase reporter carrying wild-type 3'-UTR of ZO-1 was significantly inhibited by agomir-140-3p in a dose-dependent matter ($p < 0.01$), whereas the mutation of the predicted binding site in 3'-UTR abrogated this repressive effect. These findings suggest that miR-140-3p may regulate ZO-1 expression by directly targeting the 3'-UTR of ZO-1 mRNA.

Exosomal miR-140-3p plays a significant role in Exo^{SCAD}-induced regulatory effects on ZO-1 and atherosclerotic lesion formation in a ApoE-/- mouse model.

Given the marked in vitro effects of miR-140-3p highly expressed in Exo^{SCAD} on ZO-1 expression and endothelial permeability in HAECs, we conducted in vivo studies in HFD-fed ApoE$^{-/-}$ mice. Firstly, RT-qPCR analyses of miR-140-3p expression were performed in the aortas from recipient mice treated with Exo^{SCAD}, Exo^{HC} or PBS. As a result, treatment of recipient mice with Exo^{SCAD} but not Exo^{HC} or PBS led to a robust increase in miR-140-3p expression in the aorta ($p < 0.01$, Fig. 6A). Subsequently, Exo^{SCAD} transfected with antagomir−140−3p were intravenously injected into recipient mice every 3 days for 4 weeks in the presence of continued HFD for 12 weeks. As expected, antagonism of miR−140−3p in Exo^{SCAD} reversed the effect of Exo^{SCAD} to inhibit ZO−1 (Fig. 6B). Meanwhile, the increase effect of Exo^{SCAD} on endothelial permeability was attenuated after blockade of

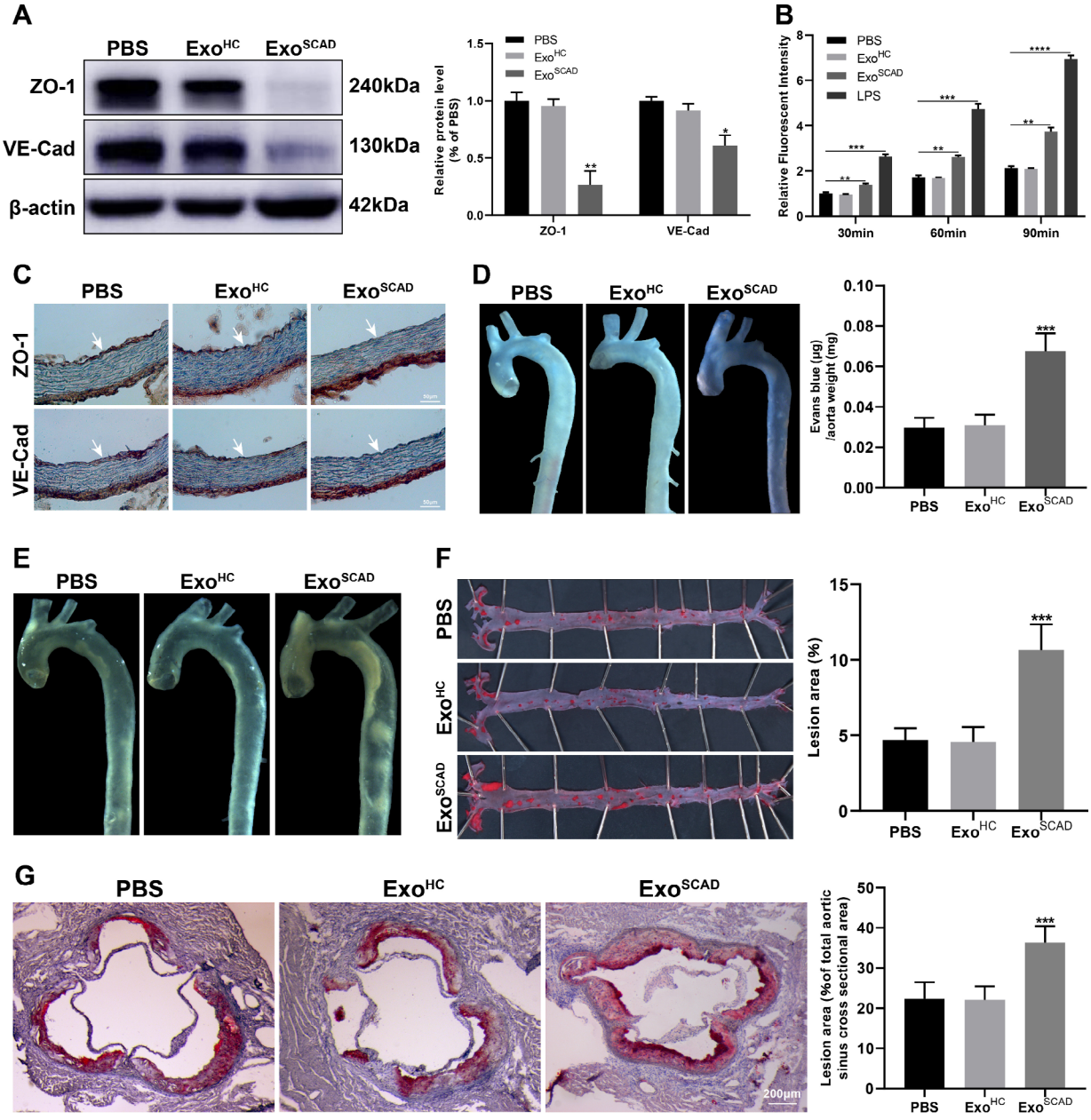

Fig. 3. Exo^{SCAD} suppress VE-Cad and ZO-1 expressions in ECs and aggravates atherosclerotic lesions. (**A**) Western blot analyses of abundance of VE-Cad and ZO-1 in HAECs treated with Exo^{SCAD}, Exo^{HC} or PBS. Representative blots (left panel) and the corresponding quantification results (right panel) of 3 replicated independent experiments. (**B**) Quantification of endothelial permeability by calculating the amount of rhodamine-dextran passing through the monolayer of HAECs treated with Exo^{SCAD}, Exo^{HC} or PBS ($n=3$ per group). LPS was used as a positive control. (**C**) Immunohistochemistry analyses of VE-Cad and ZO-1 expression in aortas from the 12-week HFD-fed ApoE$^{-/-}$ mice injected with Exo^{SCAD}, Exo^{HC} or PBS ($n=6$–10 per group). White arrows indicate tunica intima. (**D**) Representative images of aortas from the 12-week HFD-fed ApoE$^{-/-}$ mice received different treatment after intravenous injection of Evans blue in each group (left panel). Quantitation of vascular permeability by calculating the amount of Evans blue extravasated per milligram of artery in each group ($n=7$–9, right panel). (**E**) Representative bright field images of aortas from the 12-week HFD-fed ApoE$^{-/-}$ mice treated with Exo^{SCAD}, Exo^{HC} or PBS. (**F**) Representative images of the en face Oil Red O-stained aortas from the 12-week HFD-fed ApoE$^{-/-}$ mice in each group (left panel). Quantification of atherosclerotic lesion area as the percentage of positive stained areas to the respective whole arterial areas ($n=7$–9, right panel). (**G**) Representative microphotographs (left panel) and quantification (right panel) of Oil Red O-stained aortic root sections from the 12-week HFD-fed ApoE$^{-/-}$ mice in each group ($n=7$–9). Results are represented by mean ± SEM with 7–9 replicates for each group. Exo^{HC}: plasma exosomes of healthy controls; Exo^{SCAD}: plasma exosomes of patients with stable coronary artery disease; HAECs: human aortic endothelial cells; HFD: high-fat diet; LPS: lipopolysaccharide; ApoE: apolipoprotein E. $^{*}p<0.05$, $^{**}p<0.01$, $^{***}p<0.001$.

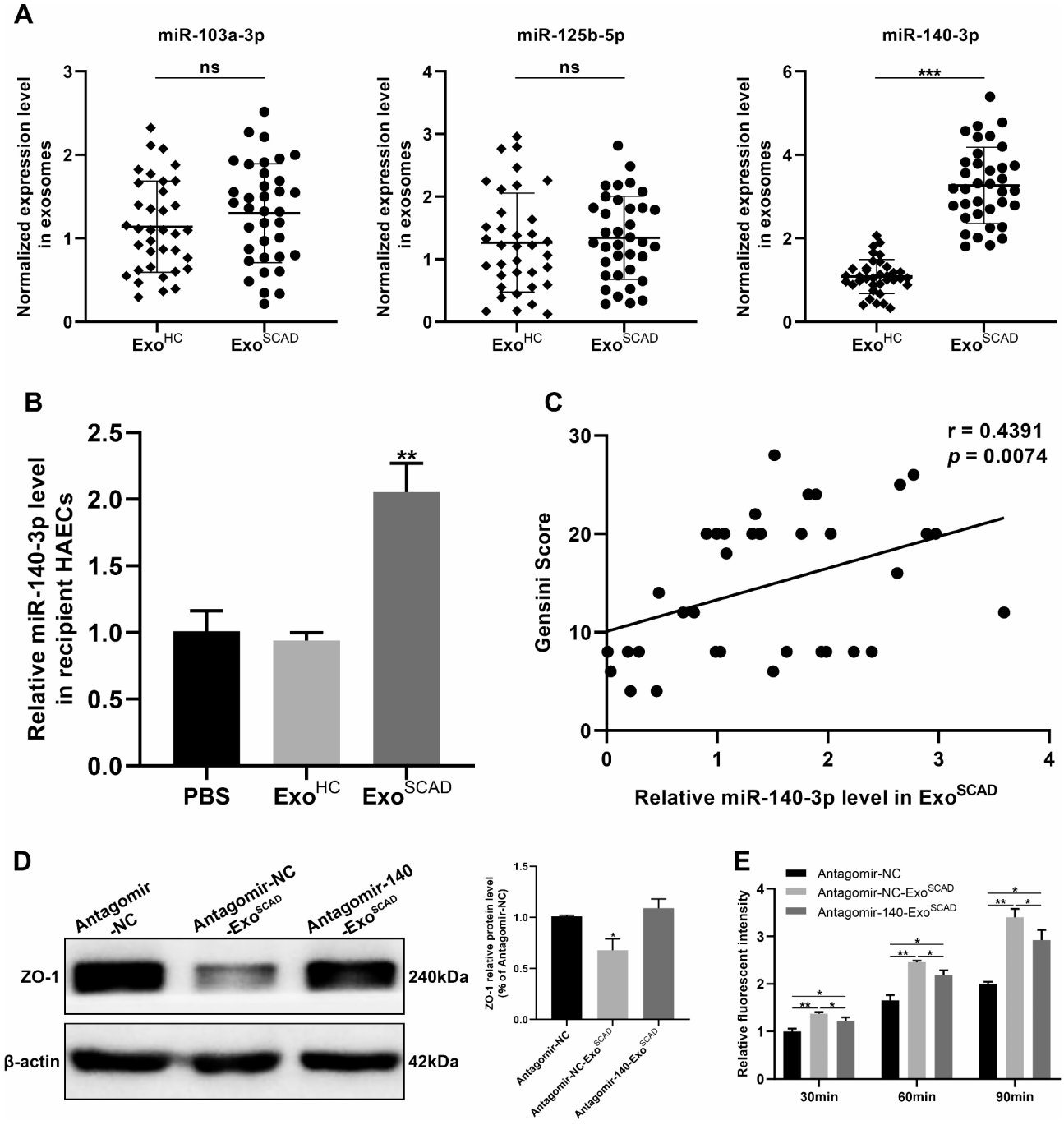

Fig. 4. Exo^{SCAD} inhibit ZO-1 expression to increase endothelial permeability via transferring highly expressed miR-140-3p into HAECs. (**A**) RT-qPCR analyses of miR-140-3p and miR-125b-5p expression in Exo^{SCAD} and Exo^{HC}. (**B**) RT-qPCR analyses of miR-140-3p expression in recipient HAECs after treatment with Exo^{SCAD}, Exo^{HC} or PBS. (**C**) Correlation of plasma exosomal miR-140-3p levels with Gensini scores in patients with SCAD. (**D**) Western blot analyses of ZO-1 expression in HAECs treated with antagomir-NC, antagomir-NC-Exo^{SCAD} or antagomir-140-Exo^{SCAD}. Representative blots (left panel) and quantification (right panel) of 3 replicated independent experiments. (**E**) Quantification of endothelial permeability by calculating the amount of rhodamine-dextran passing through the monolayer of HAECs after 30, 60, and 90 min, respectively ($n = 3$ per group). Exo^{HC}: plasma exosomes of healthy controls; Exo^{SCAD}: plasma exosomes of patients with stable coronary artery disease; HAECs: human aortic endothelial cells; agomir-140: miR-140-3p agomir; agomir-NC: agomir-140 negative control; antagomir-140: miR-140-3p antagomir; antagomir-NC: antagomir-140 negative control; antagomir-NC-Exo^{SCAD}: Exo^{SCAD} transfected with antagomir-NC; antagomir-140-Exo^{SCAD}: Exo^{SCAD} transfected with antagomir-140. $^{*}p < 0.05$, $^{**}p < 0.01$, $^{***}p < 0.001$. ns, no significance.

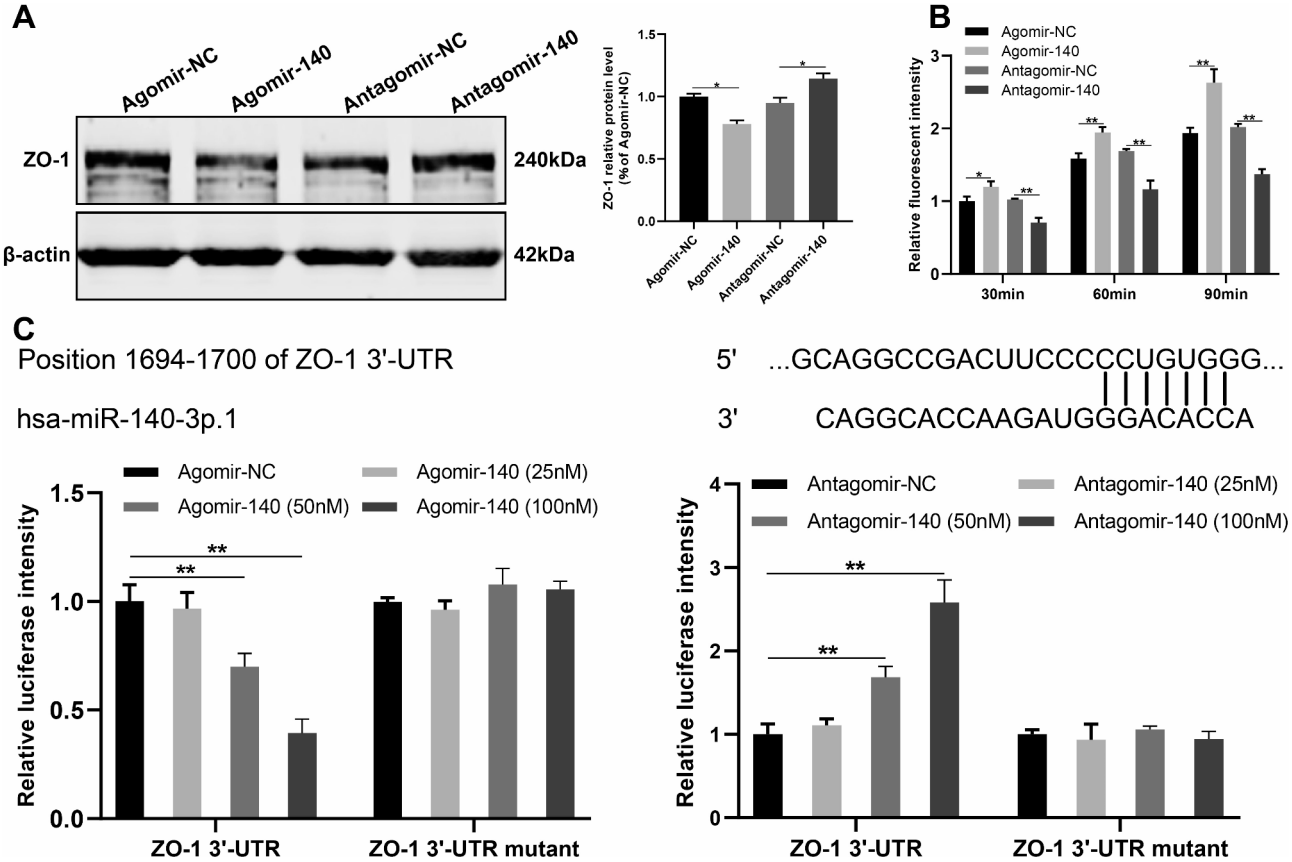

Fig. 5. miR-140-3p inhibits the expression of ZO-1 via targeting the 3'-UTR of ZO-1 mRNA to increase endothelial permeability in HAECs. (**A**) Western blot analyses of ZO-1 expression in HAECs treated with agomir-140, antagomir-140, or their NCs. Representative blots (left panel) and quantification (right panel) of 3 replicated independent experiments. (**B**) Quantification of endothelial permeability by calculating the amount of rhodamine-dextran passing through the monolayer of HAECs treated with agomir-140, antagomir-140, or their NCs ($n = 3$ per group). (**C**) miR-140-3p modulated the luciferase activity of reporter containing wild-type but not mutant 3'-UTR of ZO-1. miR-140-3p and its predicted binding sequence in the 3'-UTR of ZO-1 (upper panel). The activity of firefly luciferase reporter carrying wild-type or mutant 3'-UTR of ZO-1 after transfection with the indicated concentrations of miR-140-agomir/antagomir or their NCs (lower panel). The firefly luciferase activity was normalized to renilla luciferase activity. HAECs: human aortic endothelial cells; agomir-140: miR-140-3p agomir; agomir-NC: agomir-140 negative control; antagomir-140: miR-140-3p antagomir; antagomir-NC: antagomir-140 negative control. $^{*}p < 0.05$, $^{**}p < 0.01$. ns, no significance.

exosomal miR-140-3p ($p < 0.001$, Fig. 6C). Significantly, transfection with antagomir−140−3p ameliorated the effect of Exo^{SCAD} to accelerate atherosclerotic lesion formation ($p < 0.001$, Fig. 6D–F). Collectively, these data suggest that the suppressive effect of Exo^{SCAD} on ZO−1 expression is mediated by overexpressed exosomal miR-140-3p. In addition, miR-140-3p plays a significant role in Exo^{SCAD}-induced endothelial hyperpermeability and atherosclerotic lesion formation.

Discussion

Exosomes, which are generated by all cell types and actively secreted into various body fluids, can regulate both physiological and pathological processes and mediate various biological functions via their cargos, such as nucleic acids, proteins, lipids, and metabolites[30]. Enormous studies have indicated the crucial roles of exosomes in the regulation of ECs function. For instance, exosomes from platelets activated by von willebrand factor under high shear stress were proved to disrupt endothelial barrier function in patients with end-stage heart failure[31]. Osteocalcin-overexpressed endothelial progenitor cells-secreted exosomes reportedly promote ECs proliferation, migration and tube formation[32]. Critically, various exosomes derived from different cell types, including monocytes/macrophages, ECs, platelets and vascular smooth muscle cells, have been demonstrated to be intimately associated with atherosclerosis[33]. Enrichment of exosomes induced by adipocytes-secreted adiponectin were found to improve cardiovascular disease including atherosclerosis[34]. As depicted in Fig. 7, our findings reveal that Exo^{SCAD} could suppress VE-Cad and ZO-1 expressions in ECs to impair vascular endothelial junctions, leading to lipids and leukocytes to cross the endothelial barrier and deposit in the subendothelial layer, thereby deteriorating atherosclerosis. Notably, the decreased expression of ZO-1 is mediated by transferring of

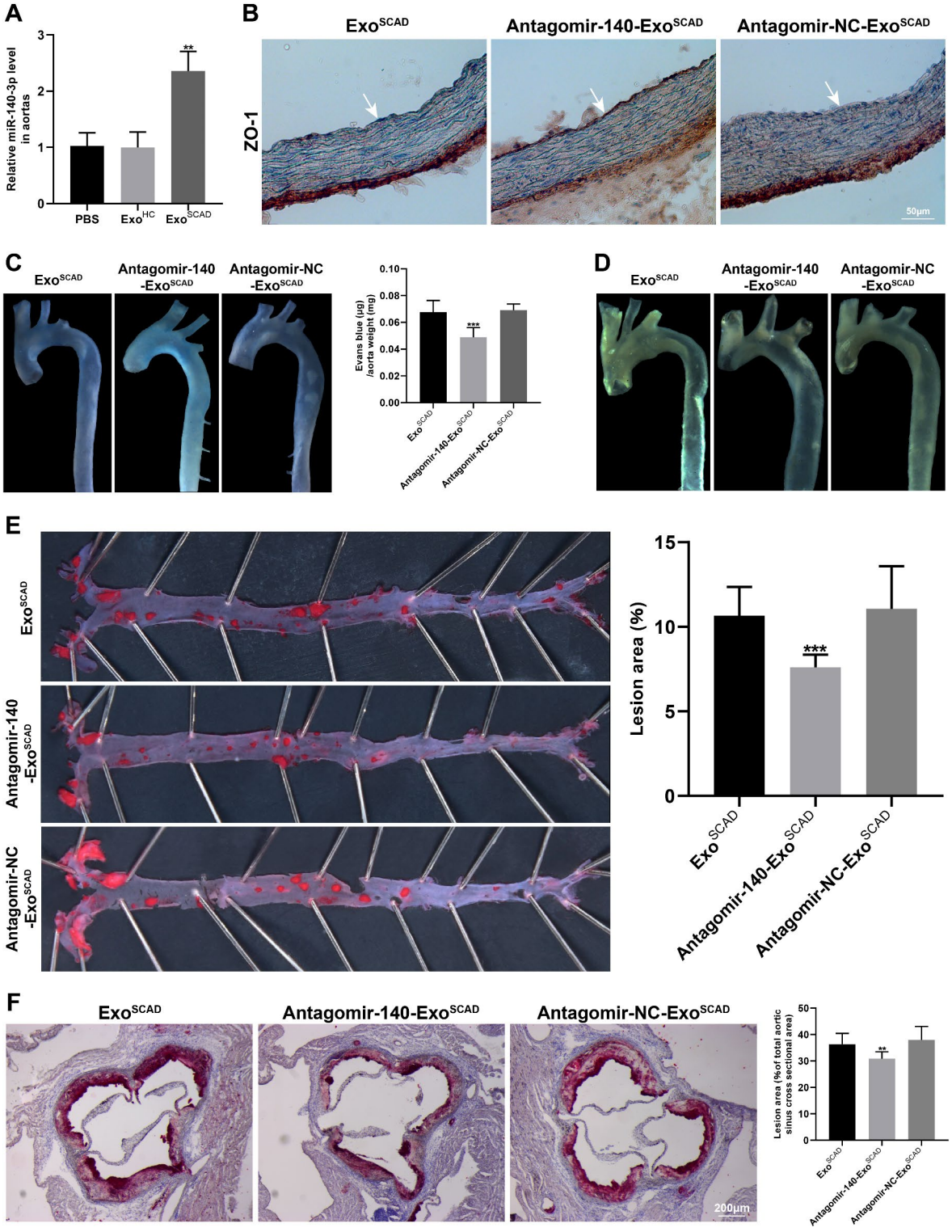

highly expressed miR-140-3p into ECs through Exo^{SCAD}. In addition, exosomal miR-140-3p has a key function in Exo^{SCAD}-induced enhancement of endothelial permeability and atherosclerotic lesion formation.

Fatty streak, caused by deposition of oxidized low-density lipoproteins (Ox-LDL) beneath the intima, is the earliest morphological change in early stage of atherogenesis[35]. Given that Ox-LDL accumulation is primarily attributed to increased vascular permeability[36,37], exploring the mechanism of endothelial hyperpermeability is therefore critical to an understanding of atherogenesis. Accumulating studies have confirmed that increased endothelial permeability resulted from impaired cell junctional proteins is the major reason for Ox-LDL to cross the endothelial barrier in early atherogenesis. The potential mechanisms underlying the endothelial hyperpermeability mediated by decreased endothelial junctions during atherosclerosis have been investigated in a limited number of studies. Researches demonstrated that Ox-LDL deposited beneath the intima and endothelial insulin-like growth factor-1 receptor deficiency enhance endothelial permeability by disrupting

◀**Fig. 6**. Exosomal miR-140-3p plays a significant role in Exo^{SCAD}-induced regulatory effects on ZO-1 and atherosclerotic lesion formation in vivo. (**A**) RT-qPCR analyses of miR-140-3p expression in the aortas from recipient mice treated with Exo^{SCAD}, Exo^{HC} or PBS. (**B**) Immunohistochemistry analyses of ZO-1 expression in aortas from the 12-week HFD-fed ApoE$^{-/-}$ mice injected with Exo^{SCAD}, antagomir-140-Exo^{SCAD} or antagomir-NC-Exo^{SCAD} ($n=7$–9 per group)). White arrows indicate tunica intima. (**C**) Representative images of aortas from the 12-week HFD-fed ApoE$^{-/-}$ mice received different treatment after intravenous injection of Evans blue in each group (left panel). Quantitation of vascular permeability by calculating the amount of Evans blue extravasated per milligram of artery in each group ($n=7$–9, right panel). (**D**) Representative bright field images of aortas from the 12-week HFD-fed ApoE$^{-/-}$ mice treated with Exo^{SCAD}, antagomir-140-Exo^{SCAD} or antagomir-NC-Exo^{SCAD}. (**E**) Representative images of the en face Oil Red O-stained aortas from the 12-week HFD-fed ApoE$^{-/-}$ mice in each group (left panel). Quantification of atherosclerotic lesion area as the percentage of positive stained areas to the respective whole arterial areas ($n=7$–9, right panel). (**F**) Representative microphotographs and quantification of Oil Red O stained aortic root sections from the 12-week HFD-fed ApoE$^{-/-}$ mice injected with Exo^{SCAD}, antagomir-140-Exo^{SCAD} or antagomir-NC-Exo^{SCAD} ($n=7$–9). Results are represented by mean ± SEM with 7–9 replicates for each group. Exo^{HC}: plasma exosomes of healthy controls; Exo^{SCAD}: plasma exosomes of patients with stable coronary artery disease; antagomir-140: miR-140-3p antagomir; antagomir-NC: antagomir-140 negative control; antagomir-NC-Exo^{SCAD}: Exo^{SCAD} transfected with antagomir-NC; antagomir-140-Exo^{SCAD}: Exo^{SCAD} transfected with antagomir-140; HFD: high-fat diet; ApoE: apolipoprotein E. $^{*}p<0.05$, $^{**}p<0.01$, $^{***}p<0.001$.

endothelial junctions in atherosclerosis[38,39]. Hemodynamics was identified to play a crucial role in the progression of atherosclerosis[40,41], research found that disturbed flow may increase endothelial permeability and promote atherosclerosis throgh disrupting VE-Cad/catenin complex[18]. Additionally, CD163 + macrophages were validated to induce endothelial hyperpermeability via suppressing VE-Cad expression in atherosclerosis[42].

Circulating exosomes have been confirmed to promote atherosclerosis by facilitating the adhesion of pro-inflammatory cells, stimulating the proliferation of vascular smooth muscle cells, and activating macrophages[43,44]. However, few researches have focused on the potential link between circulating exosomes and endothelial hyperpermeability during atherosclerosis. In this study, treatment with Exo^{SCAD} significantly decreased VE-Cad and ZO-1 expressions and enhanced endothelial permeability in HAECs. Consistent with this concept, administration of mice with Exo^{SCAD} led to downregulation of VE-Cad and ZO-1, hyperpermeability, and exacerbation of atherosclerosis in the aortas. Overall, these findings indicate an important function for Exo^{SCAD} in impairing endothelial barrier integrity and increasing endothelial permeability in the development of atherosclerosis.

Given that the filter used during exosome preparation in our study would not remove most lipoproteins, including apoB and cholesterol that are proposed to play causative roles in the development of atherosclerosis, we characterized the exosomes for presence of apoB and cholesterol. Our data revealed that apoB and cholesterol contents were similar in Exo^{HC} and Exo^{SCAD}. Combined with the fact that no significant differences in plasma low-density lipoprotein cholesterol concentration exist between the SCAD group and control group, these data eliminate the possible impact of lipoprotein and cholesterol on our overall experimental results to a certain extent.

MiRNAs have been proved to be the main biomolecules accounting for exosome-induced biological effects via negative regulation of gene expression[45]. Growing evidences have confirmed the regulatory effect of exosomal miRNAs on vascular diseases. Research showed that SOX17-induced overexpressed exosomal miR-224-5p and miR-361-3p maintain endothelial function in pulmonary hypertension via blocking the proliferation, apoptosis, and inflammation of ECs[46]. Exosomal microRNA-92a derived from cardiomyocyte was validated to be critical for post-ischemic myofibroblast activation following myocardial infarction[47]. Plasma exosomal miR-630 was identified as a crucial mediator of vascular function and cardiovascular disease risk in children with underlying obstructive sleep apnea and/or obesity[48]. Moreover, circulating exosomal miR-145 and miR-885 were indicated to play significant roles in modulating thrombosis in COVID-19[49].

Increasing researches have demonstrated that exosomes from different cells or tissues modulate atherosclerosis through delivering highly expressed miRNAs into recipient cells and tissues. For instance, adipose tissue-derived exosomal miR-132/212 and nicotine-treated macrophages-derived exosomal miR-21-3p exacerbate atherosclerosis progression by promoting migration and proliferation of vascular smooth muscle cells[50,51]. Furthermore, sleep deprivation-induced downregulation of circulating exosomal miR-182-5p and visceral adipocytes-derived exosomal miR-27b-3p aggravate endothelial inflammation and atherogenesis[14,52]. In this study, HAECs treated with Exo^{SCAD} displayed increased expression of mature miR-140-3p, decreased ZO-1 expression, and enhanced endothelial permeability. Nevertheless, an addition of exogenous antagomir-140-3p abolished the inhibitory effect of Exo^{SCAD} on ZO-1 and attenuated its effect to increase endothelial permeability. Moreover, miR-140-3p overexpression dramatically reduced ZO-1 expression and increased endothelial permeability in HAECs, whereas silencing it had the reverse effect. Luciferase assays indicated that miR-140-3p repressed ZO-1 through directly binding the 3′-UTR of ZO-1 mRNA. As predicted from our in vitro results, our in vivo studies also demonstrated that it was the miR-140-3p within the Exo^{SCAD} that caused these above-mentioned effects of Exo^{SCAD}, as evidenced by the fact that blockade of miR-140-3p in Exo^{SCAD} abrogated the inhibitory effect of Exo^{SCAD} on ZO-1 and attenuated its effect to increase endothelial permeability and exacerbate atherosclerosis in HFD-fed ApoE$^{-/-}$ mice. Additionally, pearson correlation analysis showed that exosomal miR-140–3p level coordinated with severity of SCAD. Taken together, these findings indicate

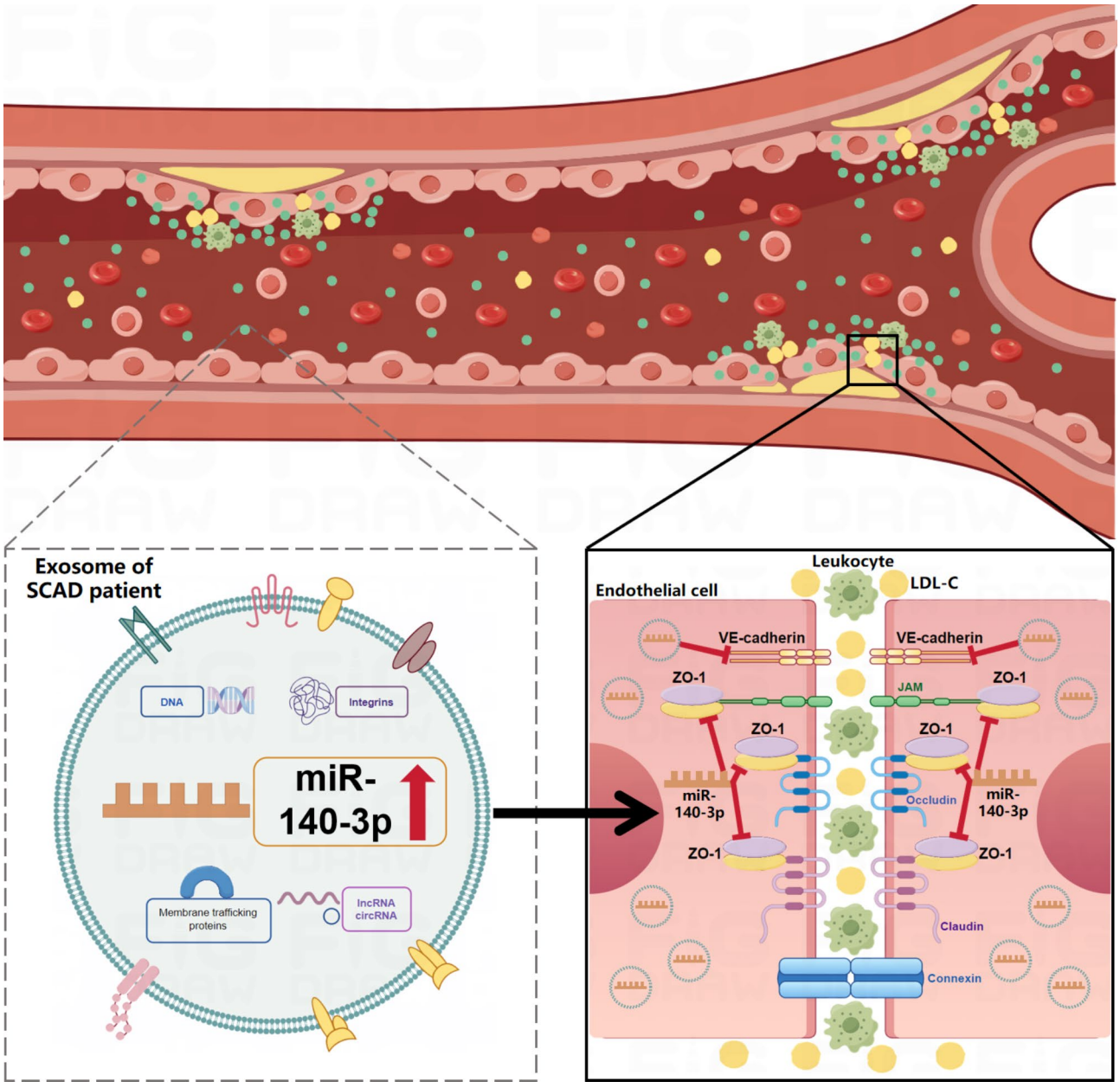

Fig. 7. Hypothesis model for the role of Exo^{SCAD} in atherosclerosis. Exo^{SCAD} suppress VE-Cad and ZO-1 expressions in endothelial cells to impair vascular endothelial junctions, leading to lipids and leukocytes to cross the endothelial barrier and deposit in the subendothelial layer, thereby deteriorating atherosclerosis. Notably, overexpressed miR-140-3p is transferred from Exo^{SCAD} into endothelial cells to inhibit ZO-1. Exo^{SCAD}: plasma exosomes of patients with stable coronary artery disease; LDL-C: low density lipoprotein cholesterol.

that Exo^{SCAD}-induced endothelial hyperpermeability via transfering of miR-140-3p into ECs to inhibit ZO-1 expression may play an crucial role in the early stage of atherosclerosis.

Interestingly, our results are supported by recent findings of similar studies about this topic. Research showed that periodontal ECs-derived exosomal miR-155-5p may deteriorate endothelial permeability and carotid atherosclerosis, accompanied by the decreased expression level of VE-Cad, ZO-1 and Claudin-1[53]. Plasma exosomal miR-129-2-3p reportedly increases airway epithelial permeability via weakening the synthesis of ZO-1, occludin, and VE-Cad in $PM_{2.5}$-aggravated asthma[54]. Beyond that, circulating exosomal miR-27b-3p and miR-375-3p were proved to augment endothelial permeability by decreasing the expression of endothelial junctional proteins, thereby accelerating circulating tumour cells metastasis[24,55].

Evidences from a number of experimental studies indicated that miR-140-3p has numerous effects including cell proliferation and migration[56,57], metabolic remodeling[58], inflammation[59,60] etc., while most researches focused on the impact of miR-140-3p on tumors. With respect to the effects of miR-140-3p on ECs, previous

studies indicated that miR-140-3p can suppress human umbilical vein ECs proliferation, migration, and tube formation through inhibiting VEGF expression[61,62]. Considering the above-mentioned potential effects of miR-140-3p, we speculate that the increased endothelial permeability via inhibiting ZO-1 appears to be an important, but likely not the only, mechanism for exosomal miR-140-3p-induced exacerbation of atherosclerosis. Furthermore, whether plasma exosomal miR-140-3p has similar effects as previously reported on arterial ECs during atherosclerosis will be the key direction in our future research.

Nevertheless, this study has several limitations. First, the exact component in Exo^{SCAD} leading to downregulation of VE-Cad in HAECs remains elusive, which needs to be determined in the future. Second, with the exception of VE-Cad and ZO-1, there might be other impaired junctional proteins that are responsible for Exo^{SCAD}-induced endothelial hyperpermeability. Additionally, apart from targeting ZO−1, miR−140 may also deteriorate endothelial permeability and atherosclerosis through other pathways, which warrants future investigation. Third, considering the genes targeted by the DEmiRNAs in Exo^{SCAD} are enriched for other functions related to atherosclerosis, inducing endothelial hyperpermeability is probably not the only factor for Exo^{SCAD} to promote atherosclerosis. In addition, given that exosomes contain a wide range of components, miRNAs may only be a risk factor rather than disease initiating for Exo^{SCAD} to exacerbate endothelial permeability and atherogenesis. Finally, the source of these plasma exosomes carrying DEmiRNAs remains unknown, which is the primary focus in our future research.

Conclusion

Altogether, we find that treatment with Exo^{SCAD} leads to decreased VE-Cad and ZO-1 expressions in ECs, endothelial hyperpermeability and aggravated atherosclerosis. Beyond that, exosomal miR-140-3p is responsible for Exo^{SCAD}-induced inhibition of ZO-1 and may be an important causative factor in the development of endothelial hyperpermeability during atherosclerosis. Notably, exosomal miR-140–3p level was positively correlated with severity of SCAD. These findings reveal the regulatory potential of miRNA-containing plasma exosomes in atherosclerosis, which may contribute to new insights into the pathogenesis of endothelial dysfunction in early atherosclerosis and open novel options for treatment of atherosclerosis.

Data availability

The data used to support the findings of this study are available from the corresponding author upon request.

Received: 2 October 2024; Accepted: 26 November 2024
Published online: 30 November 2024

References

1. Mensah, G. A., Fuster, V., Murray, C. J. L. & Roth, G. A. Global burden of cardiovascular diseases and risks, 1990–2022. *J. Am. Coll. Cardiol.* **82**(25), 2350–2473 (2023).
2. Tsao, C. W. et al. Heart disease and stroke statistics-2023 update: A report from the American heart association. *Circulation* **147**(8), e93–e621 (2023).
3. Libby, P. The changing landscape of atherosclerosis. *Nature* **592**(7855), 524–533 (2021).
4. Kalluri, R. & LeBleu, V. S. The biology function and biomedical applications of exosomes. *Science* **367**(6478), eaau6977 (2020).
5. Garcia-Martin, R. et al. MicroRNA sequence codes for small extracellular vesicle release and cellular retention. *Nature* **601**(7893), 446–451 (2022).
6. Makarova, J., Turchinovich, A., Shkurnikov, M. & Tonevitsky, A. Extracellular miRNAs and cell-cell communication: problems and prospects. *Trends Biochem. Sci.* **46**(8), 640–651 (2021).
7. Agbu, P. & Carthew, R. W. MicroRNA-mediated regulation of glucose and lipid metabolism. *Nat. Rev. Mol. Cell. Biol.* **22**(6), 425–438 (2021).
8. Wang, C. et al. Nicotine exacerbates endothelial dysfunction and drives atherosclerosis via extracellular vesicle-miRNA. *Cardiovasc. Res.* **119**(3), 729–742 (2022).
9. Mao, S. et al. Exosomal miR-141 promotes tumor angiogenesis via KLF12 in small cell lung cancer. *J. Exp. Clin. Cancer Res.* **39**(1), 193 (2020).
10. Wang, Y. et al. miR-181a, delivered by hypoxic PTC-secreted exosomes, inhibits DACT2 by downregulating MLL3, leading to YAP-VEGF-mediated angiogenesis. *Mol. Ther. Nucleic Acids*. **24**, 610–621 (2021).
11. Liu, Y. et al. Müller glia-derived exosomal mir-9-3p promotes angiogenesis by restricting sphingosine-1-phosphate receptor S1P(1) in diabetic retinopathy. *Mol. Ther. Nucleic Acids*. **27**, 491–504 (2022).
12. Liu, S. et al. M1-like macrophage-derived exosomes suppress angiogenesis and exacerbate cardiac dysfunction in a myocardial infarction microenvironment. *Basic. Res. Cardiol.* **115**(2), 22 (2020).
13. Yu, H. et al. Diabetes is accompanied by secretion of pro-atherosclerotic exosomes from vascular smooth muscle cells. *Cardiovasc. Diabetol.* **22**(1), 112 (2023).
14. Li, X. et al. Sleep deprivation promotes endothelial inflammation and atherogenesis by reducing exosomal miR-182-5p. *Arterioscler. Thromb. Vasc Biol.* **43**(6), 995–1014 (2023).
15. Ye, Z. et al. Serum exosomal microRNA-27-3p aggravates cerebral injury and inflammation in patients with acute cerebral infarction by targeting PPARγ. *Inflammation* **44**(3), 1035–1048 (2021).
16. Geng, T. et al. Exosome derived from coronary serum of patients with myocardial infarction promotes angiogenesis through the miRNA-143/IGF-IR pathway. *Int. J. Nanomed.* **15**, 2647–2658 (2020).
17. Duan, S. et al. Peripheral serum exosomes isolated from patients with acute myocardial infarction promote endothelial cell angiogenesis via the miR-126-3p/TSC1/mTORC1/HIF-1α pathway. *Int. J. Nanomed.* **17**, 1577–1592 (2022).
18. Shih, Y. T. et al. Vinculin phosphorylation impairs vascular endothelial junctions promoting atherosclerosis. *Eur. Heart J.* **44**(4), 304–318 (2023).
19. Zhou, W. et al. Targeting VEGF-A/VEGFR2 Y949 signaling-mediated vascular permeability alleviates hypoxic pulmonary hypertension. *Circulation* **146**(24), 1855–1881 (2022).
20. Yang, X. et al. Targeting endothelial tight junctions to predict and protect thoracic aortic aneurysm and dissection. *Eur. Heart J.* **44**(14), 1248–1261 (2023).
21. Mussbacher, M. et al. More than just a monolayer: the multifaceted role of endothelial cells in the pathophysiology of atherosclerosis. *Curr. Atheroscler Rep.* **24**(6), 483–492 (2022).
22. Björkegren, J. L. M. & Lusis, A. J. Atherosclerosis: recent developments. *Cell* **185**(10), 1630–1645 (2022).

23. Sun, C., Wu, M. H. & Yuan, S. Y. Nonmuscle myosin light-chain kinase deficiency attenuates atherosclerosis in apolipoprotein E-deficient mice via reduced endothelial barrier dysfunction and monocyte migration. *Circulation* **124**(1), 48–57 (2011).
24. Mao, S. et al. Exosomal mir-375-3p breaks vascular barrier and promotes small cell lung cancer metastasis by targeting claudin-1. *Transl Lung Cancer Res.* **10**(7), 3155–3172 (2021).
25. Yokota, Y. et al. Serum exosomal miR-638 is a prognostic marker of HCC via downregulation of VE-cadherin and ZO-1 of endothelial cells. *Cancer Sci.* **112**(3), 1275–1288 (2021).
26. Gao, P. et al. Pericyte-derived exosomal miR-210 improves mitochondrial function and inhibits lipid peroxidation in vascular endothelial cells after traumatic spinal cord injury by activating JAK1/STAT3 signaling pathway. *J. Nanobiotechnol.* **21**(1), 452 (2023).
27. Montalescot, G. et al. ESC guidelines on the management of stable coronary artery disease: the Task Force on the management of stable coronary artery disease of the European Society of Cardiology. *Eur. Heart J.* **34**(38), 2949–3003 (2013).
28. Ying, W. et al. Adipose tissue macrophage-derived exosomal miRNAs can modulate in vivo and in vitro insulin sensitivity. *Cell* **171**(2), 372–384 (2017).
29. Chen, G. et al. Exosomal PD-L1 contributes to immunosuppression and is associated with anti-PD-1 response. *Nature* **560**(7718), 382–386 (2018).
30. Jeppesen, D. K. et al. Reassessment of exosome composition. *Cell* **177**(2), 428–445 (2019).
31. Mone, P. et al. Exosome-mediated angiogenesis underlies LVAD-induced bleeding in patients with end-stage heart failure. *JACC Basic. Transl Sci.* **7**(3), 262–264 (2022).
32. Yi, M. et al. Exosomes secreted from osteocalcin-overexpressing endothelial progenitor cells promote endothelial cell angiogenesis. *Am. J. Physiol. Cell. Physiol.* **317**(5), C932–C941 (2019).
33. Lin, B., Yang, J., Song, Y., Dang, G. & Feng, J. Exosomes and atherogenesis. *Front. Cardiovasc. Med.* **8**, 738031 (2021).
34. Kita, S., Maeda, N. & Shimomura, I. Interorgan communication by exosomes, adipose tissue, and adiponectin in metabolic syndrome. *J. Clin. Invest.* **129**(10), 4041–4049 (2019).
35. Ginsberg, H. N. et al. Triglyceride-rich lipoproteins and their remnants: metabolic insights, role in atherosclerotic cardiovascular disease, and emerging therapeutic strategies-a consensus statement from the European Atherosclerosis Society. *Eur. Heart J.* **42**(47), 4791–4806 (2021).
36. Dejana, E., Tournier-Lasserve, E. & Weinstein, B. M. The control of vascular integrity by endothelial cell junctions: molecular basis and pathological implications. *Dev. Cell.* **16**(2), 209–221 (2009).
37. Liang, S. et al. The critical role of endothelial function in fine particulate matter-induced atherosclerosis. *Part. Fibre Toxicol.* **17**(1), 61 (2020).
38. Guo, X. et al. Reducing the damage of ox-LDL/LOX-1 pathway to vascular endothelial barrier can inhibit atherosclerosis. *Oxid. Med. Cell. Longev.* 7541411 (2022).
39. Higashi, Y. et al. Endothelial deficiency of insulin-like growth factor-1 receptor reduces endothelial barrier function and promotes atherosclerosis in apoe-deficient mice. *Am. J. Physiol. Heart Circ. Physiol.* **319**(4), H730–H743 (2020).
40. Wang, H., Uhlmann, K., Vedula, V., Balzani, D. & Varnik, F. Fluid-structure interaction simulation of tissue degradation and its effects on intra-aneurysm hemodynamics. *Biomech. Model. Mechanobiol.* **21**(2), 671–683 (2022).
41. Wang, H., Balzani, D., Vedula, V., Uhlmann, K. & Varnik, F. On the potential self-amplification of aneurysms due to tissue degradation and blood flow revealed from FSI simulations. *Front. Physiol.* **12**, 785780 (2021).
42. Guo, L. et al. CD163 + macrophages promote angiogenesis and vascular permeability accompanied by inflammation in atherosclerosis. *J. Clin. Invest.* **128**(3), 1106–1124 (2018).
43. Nikdoust, F., Pazoki, M., Mohammadtaghizadeh, M., Aghaali, M. K. & Amrovani, M. Exosomes: Potential player in endothelial dysfunction in cardiovascular disease. *Cardiovasc. Toxicol.* **22**(3), 225–235 (2022).
44. Giró, O. et al. Extracellular vesicles in atherothrombosis and cardiovascular disease: friends and foes. *Atherosclerosis* **330**, 61–75 (2021).
45. Robson, A. Exosome-derived microRNAs improve cardiac function. *Nat. Rev. Cardiol.* **18**(3), 150–151 (2021).
46. Zou, X. et al. SOX17 is a critical factor in maintaining endothelial function in pulmonary hypertension by an exosome-mediated autocrine manner. *Adv. Sci. (Weinh)* **10**(14), e2206139 (2023).
47. Wang, X., Morelli, M. B., Matarese, A., Sardu, C. & Santulli, G. Cardiomyocyte-derived exosomal microRNA-92a mediates post-ischemic myofibroblast activation both in vitro and ex vivo. *ESC Heart Fail.* **7**(1), 284–288 (2020).
48. Khalyfa, A. et al. Circulating plasma extracellular microvesicle microRNA cargo and endothelial dysfunction in children with obstructive sleep apnea. *Am. J. Respir Crit. Care Med.* **194**(9), 1116–1126 (2016).
49. Gambardella, J. et al. Exosomal miR-145 and miR-885 regulate thrombosis in COVID-19. *J. Pharmacol. Exp. Ther.* **384**(1), 109–115 (2023).
50. Guo, B. et al. MiRNA-132/212 encapsulated by adipose tissue-derived exosomes worsen atherosclerosis progression. *Cardiovasc. Diabetol.* **23**(1), 331 (2024).
51. Zhu, J. et al. Exosomes from nicotine-stimulated macrophages accelerate atherosclerosis through miR-21-3p/PTEN-mediated VSMC migration and proliferation. *Theranostics* **9**(23), 6901–6919 (2019).
52. Tang, Y. et al. Exosomal miR-27b-3p secreted by visceral adipocytes contributes to endothelial inflammation and atherogenesis. *Cell. Rep.* **42**(1), 111948 (2023).
53. Yang, W. et al. Exosomal mir-155-5p promote the occurrence of carotid atherosclerosis. *J. Cell. Mol. Med.* **28**(21), e70187 (2024).
54. Wang, C. et al. Exosomal mir-129-2-3p promotes airway epithelial barrier disruption in PM(2.5)-aggravated asthma. *J. Environ. Manage.* **370**, 123053 (2024).
55. Dou, R. et al. EMT-cancer cells-derived exosomal miR-27b-3p promotes circulating tumour cells-mediated metastasis by modulating vascular permeability in colorectal cancer. *Clin. Transl Med.* **11**(12), e595 (2021).
56. Wang, Y. et al. Circ-AASDH functions as the progression of early stage lung adenocarcinoma by targeting mir-140-3p to activate E2F7 expression. *Transl Lung Cancer Res.* **10**(1), 57–70 (2021).
57. Wang, Z. et al. Mir-140-3p is involved in the occurrence and metastasis of gastric cancer by regulating the stability of FAM83B. *Cancer Cell. Int.* **21**(1), 537 (2021).
58. Dou, D. et al. Circ_0008039 supports breast cancer cell proliferation, migration, invasion, and glycolysis by regulating the miR-140-3p/SKA2 axis. *Mol. Oncol.* **15**(2), 697–709 (2021).
59. Yang, D. et al. Extracorporeal cardiac shock wave-induced exosome derived from endothelial colony-forming cells carrying mir-140-3p alleviate cardiomyocyte hypoxia/reoxygenation injury via the PTEN/PI3K/AKT pathway. *Front. Cell. Dev. Biol.* **9**, 779936 (2021).
60. Jude, J. et al. Mir-140-3p regulation of TNF-α-induced CD38 expression in human airway smooth muscle cells. *Am. J. Physiol. Lung Cell. Mol. Physiol.* **303**(5), L460–L468 (2012).
61. Payervand, N. et al. Exosomal circ_0084043 derived from colorectal cancer-associated fibroblasts promotes in vitro endothelial cell angiogenesis by regulating the miR-140-3p/HIF-1α/VEGF signaling axis. *Heliyon* **10**(11), e31584 (2024).
62. Liang, S. et al. LncRNA SNHG1 alleviates hypoxia-reoxygenation-induced vascular endothelial cell injury as a competing endogenous RNA through the HIF-1α/VEGF signal pathway. *Mol. Cell. Biochem.* **465**, 1–11 (2020).

Acknowledgements
We thank the Key Lab of Medical Molecular Cell Biology of Shanxi Province, Institutes of Biomedical Sciences, Key Laboratory of Chemical Biology and Molecular Engineering of Ministry of Education, Shanxi University.

Author contributions
C.W. and Y.B. designed the study and revised the manuscript. C.W. supervised this study. J.H., X.K., and J.W. performed animal studies. J.H., Y.S. and X.C. conducted the in vitro experiments. X.K., Y.S. and J.W. helped to analyze the results and organize the figures. J.H. and X.K. wrote the manuscript. All authors reviewed the manuscript.

Funding
This work was supported by grants from the National Natural Science Foundation of China (grant no. 8207022039), and the Fundamental Research Program of Shanxi Province (grant no. 202203021222344).

Declarations

Competing interests
The authors declare no competing interests.

Additional information
Supplementary Information The online version contains supplementary material available at https://doi.org/10.1038/s41598-024-81352-8.

Correspondence and requests for materials should be addressed to C.W.

Reprints and permissions information is available at www.nature.com/reprints.

Publisher's note Springer Nature remains neutral with regard to jurisdictional claims in published maps and institutional affiliations.